Design and experiment verification of a new heavy friction-stir-weld robot for large-scale complex surface structures

Jiafeng Wu and Rui Zhang
School of Petroleum Engineering, China University of Petroleum, Qingdao, China, and
Guangxin Yang
Shenyang Institute of Automation, Chinese Academy of Sciences, Shenyang, China

Abstract

Purpose – This paper aims to present a new friction-stir-weld robot for large-scale complex surface structures, which has high stiffness and good flexibility.

Design/methodology/approach – The robot system is designed according to manufacturability of large aluminum products in aeronautic and astronautic area. The kinematic model of the robot is established, and a welding trajectory planning method is also developed and verified by experiments.

Findings – Experimental results show that the robot system can meet the requirements of friction stir welding (FSW) for large-scale complex surface structures.

Practical implications – Compared with other heavy robotic arm and machine tool welding devices, this robot has better working quality and capability, which can greatly improve the manufacturability for large-scale complex surface structures.

Originality/value – The friction-stir-weld robot system is a novel solution for welding large-scale complex surface structures. Its major advantages are the high stiffness, good flexibility and high precision of the robot body, which can meet the requirements of FSW. Besides, a welding trajectory planning method based on iterative closest point (ICP) algorithm is used for welding trajectory.

Keywords Friction stir welding, Heavy robot design, Large-scale complex structures

Paper type Research paper

1. Introduction

Many aerospace parts with large size and complex structure must be spliced or connected by aluminum (Al) alloy sheets using welding process, such as the tanks in heavy launch vehicle, large aircraft skin and fighter intake duct (Kumar *et al.*, 2005). To reduce the weight of aircrafts, their parts are manufactured using aerospace Al alloys, such as highly alloyed 2XXX and 7XXX series. However, it is very difficult to weld these aerospace Al alloys using the conventional fusion welding methods (Mishra and Ma, 2005).

Friction stir welding (FSW) process invented by the Welding Institute is a solid-phase connection technology (Thomas *et al.*, 1991). In FSW processing, the heat, which comes from friction between the work piece and welding tool with high-speed rotation, locally softens the material around the pin, and combination of tool rotation and translation leads to movement of material from the front of the pin to the back of the pin, and then a joint is produced in "solid state" (Mishra and Ma, 2005). Compared with fusion welding processes, the FSW process has the advantages such as low distortion and shrinkage, no fume, porosity or spatter (frequently associated with arc welding), etc. (Cook *et al.*, 2004). FSW is suitable for almost all Al alloys, and the fine microstructure in FSW produces good mechanical properties.

With the development of FSW technology and the expansion of its application area, welding joints are extended to the two-dimensional and three-dimensional contours from the long and straight shape, and higher welding precision and larger size welding joint will be required (Kumar *et al.*, 2005; Kusuda, 2013). Therefore, FSW machine with high precision and flexibility will be required with the increasing wide range of applications. Originally, FSW machine is transformed from the traditional general milling. However, load performance and power of the milling machine cannot meet the technical requirements of FSW, such as complex variety of welding joint contours, diverse materials and sizes. The world's first industrial FSW machine was manufactured by Sweden ESAB Company in 1996, which was utilized to weld Al structures

The current issue and full text archive of this journal is available on Emerald Insight at: **www.emeraldinsight.com/0143-991X.htm**

Industrial Robot: An International Journal
42/4 (2015) 332–338

[DOI 10.1108/IR-01-2015-0009]

The authors would like to thank the anonymous reviewers for valuable suggestions and corrections. This research was supported by National Science and Technology Major Project of China (Grant No. 2010ZX04007-011) and China Postdoctoral Science Foundation (Grant No. 2014M561982).

Received 8 January 2015
Revised 13 February 2015
Accepted 4 March 2015

Industrial Robot: An International Journal
Volume 42 · Number 4 · 2015 · 332–338

(Arularasu and Jothilingam, 2012). Since then, many companies have developed different types and specifications of FSW machines to meet the welding requirements of a large variety of sheets.

FSW machines can be divided into three categories according to their structural characteristics: FSW machine tool, special FSW machines and FSW robots (Cook *et al.*, 2004; Okawa *et al.*, 2006). The structure type of FSW machine tool is similar with that of machine tool, and its stiffness can meet the requirement of the FSW process, but its flexibility is not good enough. Special FSW machines are designed for a class of products, which may have the same shape, size and the material properties; the advantages of the machines include simple structure, easy controllability and good suitability for mass production. However, its disadvantage is poor flexibility. The concept of robotic FSW was presented to improve the flexibility, and heavy-duty industrial robot with high stiffness and force feedback is important for robotic FSW (Cook *et al.*, 2004; Gibson *et al.*, 2014). The FSW robots include robot arms and parallel kinematic robots (Mendes *et al.*, 2014; Shi *et al.*, 2013). The advantages of robot arms include its good flexibility, economical competition, large workspace, fast setup, etc. (Smith, 2004), and its disadvantages include low stiffness, low precision and low load capacity (Zimmer-Chevret *et al.*, 2010). Parallel kinematic robots have higher stiffness and flexibility than the robot arms, but they are not suitable for welding large-scale structure because of their small workspace.

The National Center of Advanced Manufacturing developed FSW robot for large-scale complex surface Al structures in 2002, and successfully welded the liquid oxygen tank dome of a certain commercial rocket and external fuel tank of the space shuttle and welded joints on these tanks with complex contours (Bhat *et al.*, 2001; NASA, 2008). The robot has some of the machine features, and some of the robotic features. Stiffness characteristics of the machine and flexible features of the robots are combined into this robot to perform FSW for more complex shapes and angles.

This paper proposes a new heavy friction-stir-weld robot for large-scale complex surface structures, analyzes the kinematic model of the robot and presents a welding trajectory planning method. The following sections of this paper are organized as below: the presented robot is introduced in Section 2; and the direct kinematic model is established in Section 3; the welding trajectory planning method is described in Section 4; the verification experiment is given in Section 5; and conclusion is drawn in Section 6.

2. The robot system

The new heavy friction-stir-weld robot is developed for welding certain rocket fuel tanks with the material of Al2024. The workpiece model is shown in Figure 1, which is composed of eight surface slices, one dome surface and four torus slices, with three types of weld joints, including eight curve joints, two circular joints and four longitudinal joints.

In the early experiment, the FSW process for Al2024 plates of 9.5 mm thick has been studied. The welding tool in which the pin with the diameter of 11.1 mm and the length of 8.9 mm and the shoulder with the outside diameter of 25.4 mm is used for the process test. The longitudinal feed rate along the welding joint is 90 mm/min and the spindle speed is 700 r/min. The test results are shown in Table I. According to the data in Table I, the design specifications of the presented robot can be determined.

Figure 1 The workpiece model

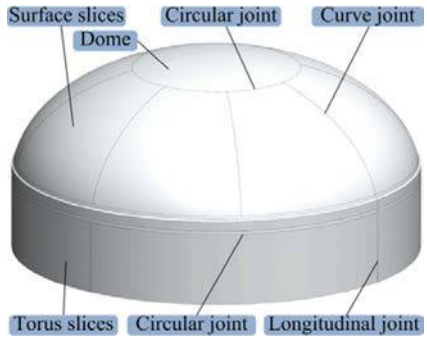

The presented robot system should be able to weld the above three types of joints. For all these joints, at least two degree of freedoms (DOFs) are required in the robot system. One is for the welding tool to be plunged into the abutting edges, and another is the rotary movement of welding tool. Besides, for circular joints, a large rotary table is also required for traverse movement of welding tool. For longitudinal joints, the robot can additionally achieve vertical movement. For curve joints, at least five DOFs are required in the robot system (including three translation DOFs and two rotation DOFs).

The robot is developed using a redundant design concept for these joints, and it is composed of three-DOF Cartesian arm, two-DOF wrist and two-DOF spindle and controlled by a Siemens Sinumeric 840D controller. The design of the robot is illustrated in Figure 2. The details are given below.

During the process of welding, axial force and welding direction traversing force and side force are all very large, there are usually thousands of Newton (see Table I). The robot should not only meet the requirement of large workspace, but also ensure the system stiffness. Therefore, the three-DOF Cartesian arm with high stiffness is chosen to enlarge the workspace of the robot. Each DOF of the arm is driven by a ball-screw-driven servomechanism along the high precision linear guides and localized by a linear encoder. Besides, the symmetrical framework is used to support vertical motion components to ensure uniform force on the robot.

The two-DOF wrist is designed to control the pose of welding tool, as shown in Figure 3. Each DOF in the wrist is realized by dual-motor drive structure, which mainly consists of two motors, two synchronous belts, a double worm mechanism and an absolute encoder. The double worm mechanism can output low speed and high torque, synchronous belts are used to reduce vibration in welding process and protect the servomotors, and absolute encoders

Table I Mechanical property for welding of AL2024

Max plunge force (kN)	Max longitudinal force (kN)	Max side force (kN)	Max spindle torque (Nm)
31.78	10.27	3.60	256

Figure 2 Design of the welding robot

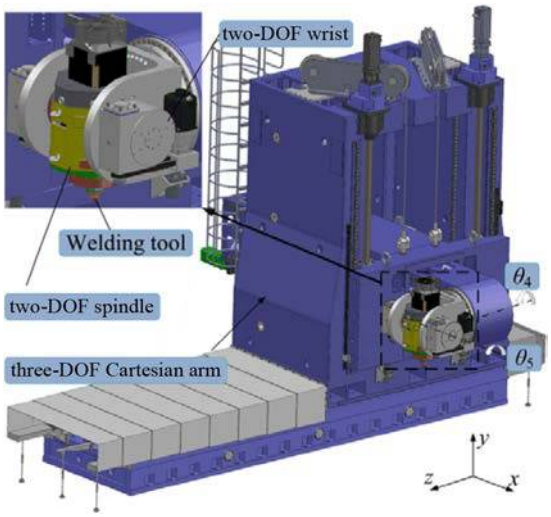

Figure 3 Design of the two-DOF wrist

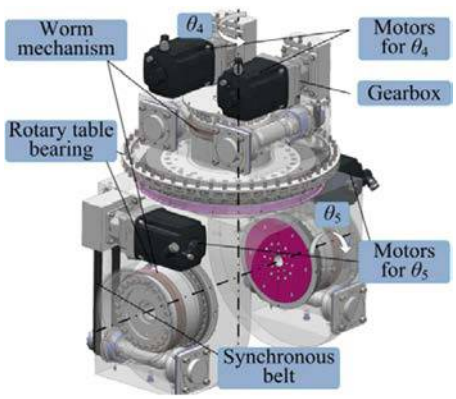

provide precise angular position feedback. With such a structure, the drive capability can be enhanced for heavy load, and the motion accuracy of the wrist can be improved using dual pinion anti-backlash drive technology (Kwon *et al.*, 2004).

The force acting on welding tool is large and the feed velocity is low while the tool is inserted into the abutting edge. If the axial motion of the tool is achieved by simultaneously controlling multi-axis of the robot, lower velocities would be assigned to each axis, and then low axial motion precision will be inevitably caused because of the stick-slip motion of feed drives, and the depth in which the shoulder plunges into the workpiece is difficult to be controlled. Small depth cannot generate enough friction, and great depth will decrease the thickness of the joint. Therefore, multi-axis control method for axial motion may be not a suitable way. To control axial motion precisely, the two-DOF spindle is developed for axial motion and rotational motion of welding tool, as shown in Figure 4, it mainly concludes three small motors for axial motion, a motor with an encoder for rotary motion, three gear pairs, a screw pair, a shaft with low thermal conductivity and welding tool. Three small motors for axial motion are used to drive three gear pairs, the screw pair and achieve axial motion

Figure 4 Design of the two-DOF spindle

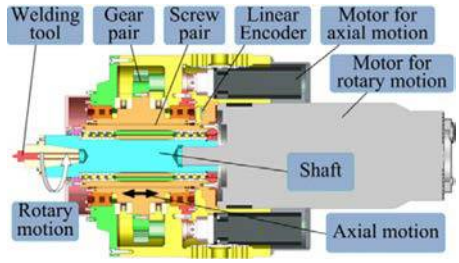

of welding tool, and the linear encoder is used to position the axial movement. The motor for rotary motion is adopted to drive the shaft directly and achieve rotary movement of welding tool, and the encoder on the motor implements stirring speed feedback. The two DOFs are independent and orthogonal.

Comparing the proposed robot design in this paper with that from NASA, 2008, the two robots are all designed for large-scale complex surface Al structures. The latter uses the 3P2R-1R manipulator configuration, the axial motion of the tool is achieved simultaneously controlling 3P2R joints of the robot, so the axial positioning accuracy of the tool is difficult to guarantee due to the stiffness of the screws, and the wear on its driver and support parts is exacerbated under high load. The former adds one DOF on the spindle for the axial motion of tool to improve the flexibility and positioning accuracy of the end effector. Besides, the main structure in the latter robot for supporting motion parts is asymmetrical, so that it would cause a great torsional deformation, and the former robot uses symmetrical structure to ensure a uniform stress on the structure.

3. Kinematic analysis

Figure 5 shows the structure of the FSW robot used in this study. In addition, The Denavit–Hartenberg parameters of the robot are given in Table II.

The forward or direct kinematics involves the motion of welding tool according to the global coordinate system. The origin of global coordinate frame (x_0, y_0, z_0) is located at the immobile base of the robot (see Figure 2). Each of the robot DOFs is modeled, and each model can be described as the homogeneous transformation matrix ${}_iT$, which uses four link parameters (Rigelsford, 2003). This transformation is known as the Denavit–Hartenberg notation:

Figure 5 Coordinate systems of the robot

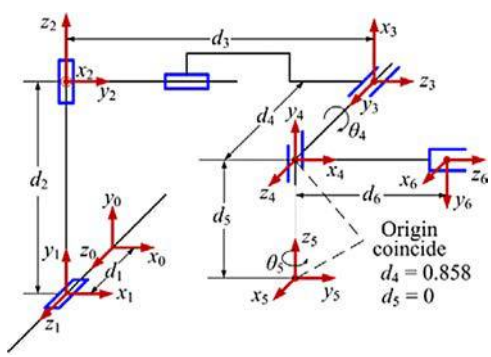

Table II DH parameters of the FSW robot

Joint i	α_{-1}(rad)	a_{-1}(m)	θ_i(rad)	d_i (m)
1	0	0	0	d_1 (0)
2	$-\pi/2$	0	$-\pi/2$	d_2 (0)
3	$-\pi/2$	0	$-\pi/2$	d_3 (0)
4	$-\pi/2$	0	$\theta_4(-\pi/2)$	0.858
5	$-\pi/2$	0	$\theta_5(-\pi/2)$	0
6	$-\pi/2$	0	0	d_6 (0.55)

$$ {}^{i-1}_{i}\boldsymbol{T} = Rot(x,\alpha_{i-1})\,Trans(x,\alpha_{i-1})\,Rot(z,\theta_i)\,Trans(z,d_i) \quad (1) $$

where α_{i-1} is the offset angle from the z_{i-1} axis to the z_i axis about the x_{i-1} axis, a_{i-1} is the offset distance from the z_{i-1} axis to the z_i along the x_{i-1} axis. θ_i is the joint angle from the x_{i-1} axis to the x_i axis about z_i axis, and d_i is the distance from the x_{i-1} axis to the x_i axis along z_i axis. Therefore, the position and orientation matrix of the welding tool of the robot according to the global coordinate system can be obtained as following:

$$ {}^{0}_{6}\boldsymbol{T} = \prod_{i=1}^{6} {}^{i-1}_{i}\boldsymbol{T} = \begin{bmatrix} -s\theta_4c\theta_5 & c\theta_4 & s\theta_4c\theta_5 & d_6s\theta_4s\theta_5 + d_3 \\ c\theta_4c\theta_5 & s\theta_4 & -c\theta_4s\theta_5 & -d_6c\theta_4s\theta_5 + d_2 \\ -s\theta_5 & 0 & -c\theta_5 & -d_6c\theta_5 + d_1 + d_4 \\ 0 & 0 & 0 & 1 \end{bmatrix} \quad (2) $$

4. Welding trajectory planning

As shown in Figure 6, welding trajectory for three-dimensional contours can be described as a set of points $\boldsymbol{P} = \{\boldsymbol{P_i} \in R^{3\times 1}, i = 0\ [\ldots], n+1\}$ and a set of unit vectors $\boldsymbol{n} = \{\boldsymbol{n_i} \in R^{3\times 1} \mid \boldsymbol{n_0} = \boldsymbol{n_1}, \boldsymbol{n_n} = \boldsymbol{n_{n+1}}, i = 0\ [\ldots], n+1\}$. The robot's movement is given below. First, rapidly feed welding tool to the point $\boldsymbol{P_0}$ and make the spindle direction coinciding with $\boldsymbol{n_0}$. Second, lock the first to the fifth robot joints, start up the sixth joint and spindle rotary motion and make welding tool plunge the welded seam to $\boldsymbol{P_1}$. Third, lock the motor of the sixth robot joint, start up the first to the fifth robot joints and move welding tool along the welded seam at traverse speed F. Finally, after welding tool arrives at $\boldsymbol{P_n}$, start up the sixth robot joint and draw welding tool back to the point $\boldsymbol{P_{n+1}}$. The method of determining $\boldsymbol{P}$ and $\boldsymbol{n}$ is given below.

Figure 6 The welding trajectory schemes

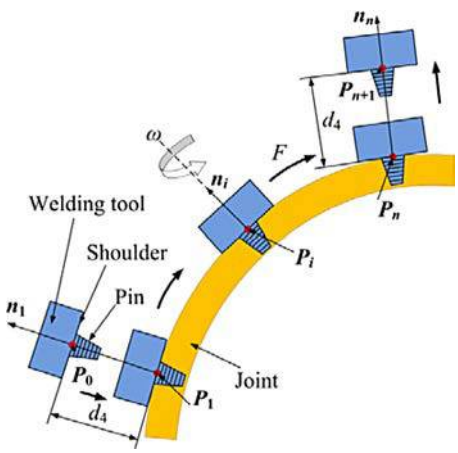

As the workpiece is arbitrarily mounted on the rotary table, the error between the planned and the actual trajectory of the welding joint is introduced, as illustrated in Figure 7. The planned trajectory can be described by the positions $\boldsymbol{Q} = \{\boldsymbol{Q_i} \in R^{3\times 1}, i = 1\ [\ldots], n\}$ and the unit normal vector $\boldsymbol{N} = \{\boldsymbol{N_i} \in R^{3\times 1}, i = 1\ [\ldots], n\}$ of welding surface at $\boldsymbol{Q_i}$. We require a 3×3 rotation matrix $\boldsymbol{R}$ and a 3×1 translation matrix $\boldsymbol{p}$ that represent the rotation and translation of the welding joint from its planned trajectory to its actual trajectory, and the actual trajectory can be obtained as following:

$$ (\boldsymbol{P}_i, \boldsymbol{n}_i) = (\boldsymbol{RQ}_i + \boldsymbol{p}, \boldsymbol{RN}_i) \quad (3) $$

There are many methods to solve the two matrices $\boldsymbol{R}$ and $\boldsymbol{p}$, such as the iterative closest point (ICP) algorithm (Besl and McKay, 1992), variation algorithm (Chatelain, 2005), tangent algorithm (Chu *et al.*, 1997) and Hong-Tan algorithm (Hong and Tan, 1993). All these algorithms can converge successfully to global minima when the orientational error does not exceed certain range, and the ICP algorithms have slightly better robustness property than the other algorithms (Li *et al.*, 1998). Besides, compared with the other algorithms, the ICP algorithms were more widely used for the field of surface reconstruction, object recognition and localization. In this paper, we will use the ICP algorithm to solve the transformation matrices. Let $\boldsymbol{Y} = \{\boldsymbol{y_i} \in R^3, i = 1, 2, \ldots, n\}$ is measurement points on welding joint, and $\boldsymbol{X} = \{\boldsymbol{x_i} \in R^3 \mid x_i = \Phi(u_i, v_i), i = 1, 2, \ldots, n\}$ is the points on the surface model corresponding with $\boldsymbol{Y}$, and $\boldsymbol{n'_i}$ is the unit normal the workpiece surface at $\boldsymbol{x_i}$. Then, the objective function for $(\boldsymbol{R}, \boldsymbol{p})$ can be described as:

$$ \varepsilon = \min f(\boldsymbol{R}, \boldsymbol{p}, \boldsymbol{x}, \boldsymbol{n}') = \sum_{i=1}^{n} \|\langle \boldsymbol{R}^{-1}\cdot(\boldsymbol{y}_i - \boldsymbol{p}) - \boldsymbol{x}_i, \boldsymbol{n}'_i\rangle\|^2 \quad (4) $$

The orientation matrix $\boldsymbol{R}$ can also be expressed by quaternion as follows:

$$ \boldsymbol{R}(\boldsymbol{q}) = \begin{bmatrix} q_0^2 + q_1^2 - q_2^2 - q_3^2 & 2(q_1q_2 + q_0q_3) & 2(q_1q_3 - q_0q_2) \\ 2(q_1q_2 - q_0q_3) & q_0^2 - q_1^2 + q_2^2 - q_3^2 & 2(q_2q_3 + q_0q_1) \\ 2(q_1q_3 + q_0q_2) & 2(q_2q_3 - q_0q_1) & q_0^2 - q_1^2 - q_2^2 + q_3^2 \end{bmatrix} \quad (5) $$

Where $\boldsymbol{q} = (q_0, q_1, q_2, q_3) \in [0,1]$, and $\|\boldsymbol{q}\| = 1$.

The steps for solving $\boldsymbol{R}$ and $\boldsymbol{p}$ are detailed below:

- *Step 0*: Calculate $\bar{y} = 1/n\sum y_i$, $\bar{x} = 1/n\sum x_i^k$;
- *Step 1*: Calculate $w = \sum(y_i - \bar{y})(x_i - \bar{x})^T$;

Figure 7 Solution of the modified trajectory

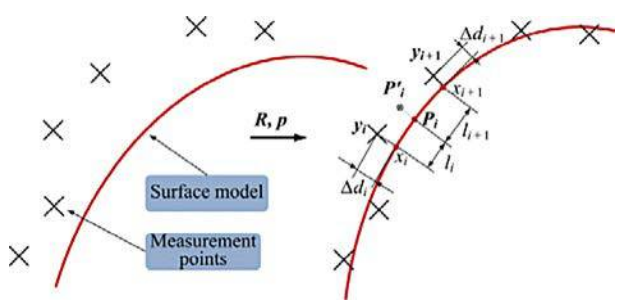

- *Step 2*: Calculate $N(w) = \begin{bmatrix} tr(w) & w^T - w \\ w - w^T & w + w^T - tr(w)\boldsymbol{I} \end{bmatrix}$, where $tr(w)$ describes the trace of a matrix w and $\boldsymbol{I}$ is the identity matrix.
- *Step 3*: Calculate the eigenvector $\boldsymbol{q}^k$ of the matrix $\boldsymbol{N}(\boldsymbol{w})$ corresponding to maximum eigenvalue.
- *Step 4*: Update the matrix $\boldsymbol{R}^k(\boldsymbol{q}^k)$, $\boldsymbol{p}^k = \bar{\boldsymbol{y}} - \boldsymbol{R}^k \bar{\boldsymbol{x}}^k$.

Due to the manufacturing errors or the deformations of the workpiece, the actual trajectory cannot coincide with measurement points $\boldsymbol{M}$, which will lead to uneven plunge depth during welding process. Therefore, it should modify the actual trajectory with reference to the measurement data. Set the modified trajectory as $\boldsymbol{P}' = \{\boldsymbol{P}'_i \in \mathrm{R}^{3\times 1}, i = 1\ [\ldots], n\}$, and the unit vectors at the points $\boldsymbol{P}'$ is also equal to $\boldsymbol{n}$. Thus, $\boldsymbol{P}'$ can be obtained:

$$\boldsymbol{P}'_i = \boldsymbol{P}_i + \left(\frac{l_{i+1}\Delta d_i + l_i \Delta d_i}{l_i + l_{i+1}} - d_{plunge}\right)\boldsymbol{n}_i \tag{6}$$

where Δd_i is the distance from $\boldsymbol{y}_i$ to the actual trajectory, and l_i is the distance between $\boldsymbol{P}_i$ and $\boldsymbol{x}_i$ and d_{plunge} is the depth that shoulder plunges into workpiece (see Figure 7).

Based on equation (2), we can obtain:

$$\boldsymbol{n} = \begin{pmatrix} n_1 \\ n_2 \\ n_3 \end{pmatrix} = -\begin{pmatrix} s\theta_4 s\theta_5 \\ -c\theta_4 s\theta_5 \\ -c\theta_5 \end{pmatrix} \boldsymbol{P}' = \begin{pmatrix} P'_1 \\ P'_2 \\ P'_3 \end{pmatrix} = \begin{pmatrix} d_6 s\theta_4 s\theta_5 + d_3 \\ -d_6 c\theta_4 s\theta_5 + d_2 \\ -d_6 c\theta_5 + d_1 + d_4 \end{pmatrix} \tag{7}$$

The joint angles can be computed for any given global Cartesian coordinate system in an industrial application. Solve equation (7), the result is:

$$\begin{cases} \theta_4 = a\tan 2(-n_1, n_2) \\ \theta_5 = -a\cos(n_3) \\ d_4 = 0.858 \\ d_6 = 0.55 + D \\ d_1 = P'_3 - d_4 + d_6\cos\theta_5 \\ d_2 = P'_2 + d_6\cos\theta_4\sin\theta_5 \\ d_3 = P'_2 - d_6\sin\theta_4\sin\theta_5 \end{cases} \tag{8}$$

Figure 8 The presented robot prototype

These modified coordinate points can be input into the control system, and welding tool is controlled to move along the planned trajectory.

5. Experimental results

A prototype was fabricated to test the performance of the designed robot, as illustrated in Figure 8. The main parameters of our robot are shown in Table III. The prototype will be used for the following experiment. From Figure 8, the experiment system also includes a rotary table and a fixture for workpiece clamping. In the experiment, we will investigate whether the robot can weld large-scale complex structures. Furthermore, we will evaluate whether the proposed welding trajectory planning method is feasible.

As shown in Figure 9, two complex surface structures with same thickness are selected and placed on the fixture for welding experiment, with the thickness of 5.5 mm and the material of Al2024. The workpiece model in the robot coordinate system is described as follows.

$$\left(\frac{x}{1670}\right)^2 + \left(\frac{y}{1050}\right)^2 + \left(\frac{z}{1670}\right)^2 = 1, (x < 0, y > 0) \tag{9}$$

The position of welding seam can be measured by the robot. The probe TS220 made by HEIDENHAIN is used to measure the coordinate of welding seam. Before measuring, the probe is mounted on the spindle, and two-DOF wrist and the spindle are placed in the initial position, while the three-DOF arm is only controlled to measure 30 points along the welding seam. As shown in Figure 10, the measurement points and the workpiece model based on equation (9) are plotted in the robot coordinate system. Based on the proposed method described in Section 4, and the matrix $(\boldsymbol{R}, \boldsymbol{p})$ in equation (4) is solved:

$$(\boldsymbol{R}, \boldsymbol{p}) = \begin{pmatrix} 0.9932607 & -0.0866893 & -0.0769301 & 1903.85 \\ 0.0847772 & 0.9960124 & -0.0277886 & 1761.42 \\ 0.0790323 & 0.0210795 & 0.9966492 & 117.35 \end{pmatrix} \tag{10}$$

Matching results from its planned trajectory to its actual trajectory are shown in Figure 11. The maximum deviation errors between measurement points and CAD model is up to 2.15 mm. Therefore, the planned welding trajectory is modified based on equation (6), and the modified data are input into the control system for welding.

Welding parameters in the experiment are shown in Table IV, and welding result is shown in Figure 12. From Figure 12, it can be noted that there is good weld quality and uniform plunge depth. The experiment shows that the robot can meet the welding requirement of the large-scale complex surface structure, and also verifies that the presented welding trajectory planning method is feasible.

Table III The main parameters of the robot

Joint *i*	1	2	3	4	5	6
Workspace	0~3.5 m	0~1.8 m	0~1.6 m	−195°~−85°	−110°~−70°	0~0.05 m
Feed speed	1.25 m/min	1.25 m/min	1.25 m/min	2 r/min	2 r/min	0.2 m/min

Figure 9 Workpiece mounted on the fixture

Figure 10 Workpiece model and measurement points

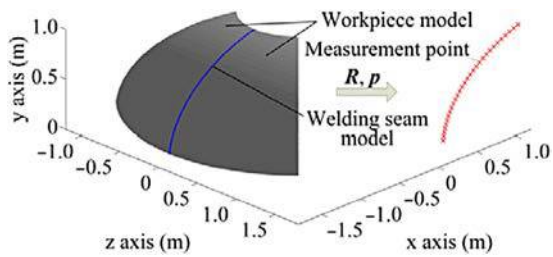

Figure 11 Matching result

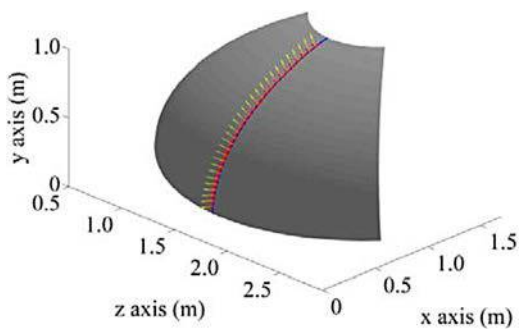

Table IV Welding parameters in the experiment

Rotation speed (r/min)	Welding speed (mm/min)	Axial depth (mm)
800	80	0.3

6. Conclusions

In this paper, a new heavy friction-stir-weld robot is introduced for large-scale complex surface structures, and the robot consists of three-DOF Cartesian arm, two-DOF wrist and two-DOF spindle. Two-DOF spindle achieves rotary movement and feed movement that welding tool plunges into workpiece, and welding traverse for three-dimensional contours is achieved by three-DOF Cartesian arm and two-DOF wrist. Second, the direct kinematics of the robot is established, and a welding trajectory planning method is presented based on the kinematics model. In the method, the measured points and CAD model of the workpiece is aligned using the ICP algorithm, and then the actual trajectory is modified using the measured points. Finally, the prototype is fabricated to test performance of the robot, and the experiment results show that the presented robot can weld large-scale three-dimensional space complex structure, and the presented welding trajectory planning method is correct and feasible. It believes that the newly developed robot can be applied for welding large and complex welded Al structure in the aerospace area.

In future work, we are going to improve the robot's autonomy in two ways. First, seam-tracking system will be added into the system. Second, force sensor and torque sensor will be added on the two-DOF spindle to achieve force-position hybrid control of the robot.

Figure 12 The welded workpiece

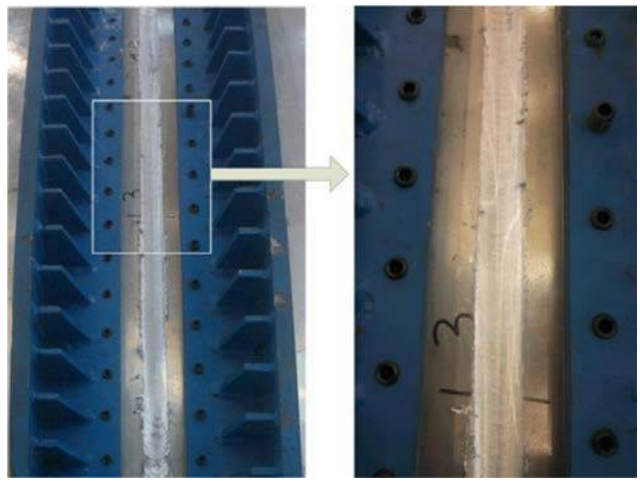

References

Arularasu, S. and Jothilingam, A. (2012), "Design and development of low cost friction stir welding machine", *2012 International Conference on Advances in Engineering, Science and Management (ICAESM)*, IEEE, Nagapattinam, pp. 305-311.

Besl, P.J. and McKay, N.D. (1992), "A method for registration of 3-D shapes", *Robotics-DL Tentative: International Society for Optics and Photonics*, Vol. 14 No. 2, pp. 586-606.

Bhat, B.N., Carter, R.W., Ding, R.J., Lawless, K.G., Nunes Jr, A.C., Russell, C.K. and Shah, S.R. (2001), *Friction Stir Welding Development at NASA-Marshall Space Flight Center*, available at: http://ntrs.nasa.gov/archive/nasa/casi.ntrs.nasa.gov/20020015869.pdf

Chatelain, J.-F. (2005), "A level-based optimization algorithm for complex part localization", *Precision Engineering*, Vol. 29 No. 2, pp. 197-207.

Chu, Y., Gou, J., Kang, B., Woo, K. and Li, Z. (1997), "Performance analysis of localization algorithms", *Proceedings IEEE International Conference on Robotics and Automation*, IEEE, *Albuquerque, NM*, pp. 1247-1252.

Cook, G.E., Crawford, R., Clark, D.E. and Strauss, A.M. (2004), "Robotic friction stir welding", *Industrial Robot: An International Journal*, Vol. 31 No. 1, pp. 55-63.

Gibson, B., Lammlein, D., Prater, T., Longhurst, W., Cox, C., Ballun, M., Dharmaraj, K., Cook, G. and Strauss, A. (2014), "Friction stir welding: process, automation, and control", *Journal of Manufacturing Processes*, Vol. 16 No. 1, pp. 56-73.

Hong, J. and Tan, X. (1993), "Method and apparatus for determining position and orientation of mechanical objects", US Patent 5208763.

Kumar, B., Widener, C., Jahn, A., Tweedy, B., Cope, D. and Lee, R. (2005), "Review of the applicability of FSW processing to aircraft applications", 46th AIAA SDM Conference, Austin, TX.

Kusuda, Y. (2013), "Honda develops robotized FSW technology to weld steel and aluminum and applied it to a mass-production vehicle", *Industrial Robot: An International Journal*, Vol. 40 No. 3, pp. 208-212.

Kwon, Y., Hwang, H.Y., Lee, H. and Kim, S. (2004), "Rate loop control based on torque compensation in anti-backlash geared servo system", *Proceedings of the 2004 American Control Conference*, IEEE, *Boston, MA*, pp. 3327-3332.

Li, Z., Gou, J. and Chu, Y. (1998), "Geometric algorithms for workpiece localization", *IEEE Transactions on Robotics and Automation*, Vol. 14 No. 6, pp. 864-878.

Mendes, N., Neto, P., Simão, M., Loureiro, A. and Pires, J. (2014), "A novel friction stir welding robotic platform: welding polymeric materials", *The International Journal of Advanced Manufacturing Technology*, Barcelona, pp. 1-10.

Mishra, R.S. and Ma, Z. (2005), "Friction stir welding and processing", *Materials Science and Engineering: R: Reports*, Vol. 50 No. 1, pp. 1-78.

NASA (2008), "MSFC large-scale manufacturing", available at: www.nasa.gov/sites/default/files/files/LargeScaleMfg.pdf

Okawa, Y., Taniguchi, M., Sugii, H. and Marutani, Y. (2006), "Development of 5-axis friction stir welding system", *International Joint Conference on SICE-ICASE*, *IEEE, Busan*, pp. 1266-1269.

Rigelsford, J. (2003), "Fundamentals of robotic mechanical systems", *Industrial Robot: An International Journal*, Vol. 30 No. 6.

Shi, J., Wang, Y., Zhang, G. and Ding, H. (2013), "Optimal design of 3-DOF PKM module for friction stir welding", *The International Journal of Advanced Manufacturing Technology*, Vol. 66 Nos 9/12, pp. 1879-1889.

Smith, C.B. (2004), "Robotic friction stir welding using a standard industrial robot", *Journal of Light Metal Welding and Construction*, Vol. 42 No. 3, pp. 40-41.

Thomas, W., Nicholas, E., Needham, J., Murch, M., Templesmith, P. and Dawes, C. (1991), "International patent application number PCT/GB92/02203 and GB Patent Application number 9125978.9", *PCT/GB92, patent application*, (9,125,978.8).

Zimmer-Chevret, S., Langlois, L., Laye, J., Goussain, J.-C., Martin, P. and Bigot, R. (2010), "Determining the ability of a high payload robot to perform FSW applications", 8th International Symposium on Friction Stir Welding, Lübeck.

Corresponding author

Jiafeng Wu can be contacted at: hitwu@163.com